Hindawi Publishing Corporation
International Journal of Antennas and Propagation
Volume 2016, Article ID 5961309, 11 pages
http://dx.doi.org/10.1155/2016/5961309

Research Article

Pattern Reconfigurable Wideband Stacked Microstrip Patch Antenna for 60 GHz Band

Alexander Bondarik and Daniel Sjöberg

Department of Electrical and Information Technology, Lund University, Box 118, 221 00 Lund, Sweden

Correspondence should be addressed to Alexander Bondarik; alexander.bondarik@eit.lth.se

Received 18 September 2015; Revised 30 December 2015; Accepted 10 January 2016

Academic Editor: Giuseppe Castaldi

A beam shift method is presented for an aperture coupled stacked microstrip antenna with a gridded parasitic patch. The gridded parasitic patch is formed by nine close coupled identical rectangular microstrip patches. Each of these patches is resonant at the antenna central frequency. Using four switches connecting adjacent parasitic patches in the grid, it is possible to realize a pattern reconfigurable antenna with nine different beam directions in broadside, H-plane, E-plane, and diagonal planes. The switches are modeled by metal strips and different locations for strips are studied. As a result an increase in the antenna coverage is achieved. Measurement results for fabricated prototypes correspond very well to simulation results. The antenna is designed for 60 GHz central frequency and can be used in high speed wireless communication systems.

1. Introduction

The high frequency associated with millimeter-waves provides high isolation between neighboring networks due to the free space loss. This fact is further enhanced by rain attenuation in outdoor links, and the oxygen absorption peak at 60 GHz, though this is of little impact for short range scenarios (<50 m) [1]. A wide bandwidth (up to 7 GHz) is available worldwide around the mentioned frequency and recently more and more applications are utilizing 60 GHz escaping from highly exploited lower frequencies [2]. However, to compensate the propagation attenuation, high gain antennas are needed. The narrow beam width for these antennas limits the communication directions and a beam control can solve this problem to a certain extent [3]. As an example, the 60 GHz band is considered to be used for millimeter-wave backhaul systems in a mobile network. These systems are mounted outdoors and work under a line-of-sight condition. Environmental circumstances, such as wind and temperature gradient, cause antennas misalignment, which can reach 5° amplitude [4].

A traditional solution using a phased array antenna with phase shifters is usually expensive and complex, which is not suitable for mass market commercial applications. An alternative is a reconfigurable antenna where the beam shift can be realized by modifying the geometry using control elements. A number of papers have been published to report reconfigurable microstrip patch antennas. However the majority are designed to operate at a few GHz frequencies. In [5] a beam shift technique using parasitic patches was introduced. A beam shift in the E-plane was achieved by connecting parasitic patches to the ground. The weakness of the described realization was low gain. The same idea was used in [6] where four parasitic patches were arranged symmetrically around a driven element. Different combinations of parasitic patches connections to the ground allowed achieving nine beam positions, however with quite low antenna efficiency. In [7] a microstrip patch design surrounded by microstrip rings was described. Using combinations of connections to the ground a beam steering was achieved in the H-plane and in the E-plane. The drawback of the proposed design was big variations of gain for different beams. In [8] a stacked microstrip antenna design was introduced, where a rectangular grid of nine close coupled electrically small rectangular metallic pixels was coupled to a driven rectangular patch. By connecting and disconnecting pixels in the grid using p-i-n diodes, a beam shift in nine directions was realized.

In [9] the antenna design described in [8] was implemented for 60 GHz central frequency. The interconnections were realized by metal strips. However, only simulation results were presented. In [10] a prototype of a reconfigurable quasi-Yagi antenna design for the 60 GHz band was described. In [11] a pattern reconfigurable patch antenna array was presented for 60 GHz. In the described antenna a patch was connected to a microstrip line stub shortened to a ground plane. A p-i-n diode was used to alter the length of the stub and to change the excitation phase of the patches. The reported antenna bandwidth was narrow and corresponded to a single patch antenna bandwidth.

In this paper a beam shift realization is presented for a novel stacked microstrip patch antenna first reported in [12]. In contrast to lower frequency designs presented in [5–7] the proposed antenna has a multilayer structure to achieve a wide bandwidth specification for 60 GHz wireless systems. The antenna consists of an aperture coupled driven patch and a parasitic gridded patch on the antenna top layer. The gridded patch is composed of nine close coupled rectangular patches resonant at a central frequency. The antenna has a double resonance behavior and 22% measured impedance bandwidth. This differs the proposed antenna from the lower frequency realization described in [8] where nonresonant metal pixels compose the parasitic layer; the antenna has a single resonance behavior and 6% measured impedance bandwidth. In [9] a different antenna feeding as well as increased substrate thickness with air gap is implemented for the 60 GHz antenna with pixels on the parasitic layer. Although reported simulated impedance bandwidth is wider than in [8], it is difficult to judge the antenna without measurement confirmation.

The pattern reconfigurability property is realized by connecting adjacent patches on the top layer. The connections are modeled by metal strips. Comparing to the realizations in [5–7] where parasitic patches were connected to a ground, the antenna top layer connections are much easier to realize at 60 GHz, especially for a multilayer antenna structure. Comparing to [8, 9] the number of used interconnections is less.

In the proposed design nine different beam directions in broadside, H-plane, E-plane, and diagonal plane are realized using four switches. All eight shifted beams have wider beam width compared to the broadside direction beam for the reference antenna without beam shift. This results in the considerable increase of beam coverage solid angle for the reconfigurable antenna compared to the reference antenna. The reconfigurable antenna preserves wide return loss bandwidth, with about 1 dB gain difference for nine beam realizations. The antenna prototype was fabricated and measured. Experimental results are in good agreement with simulations. It is the first paper for a wideband reconfigurable microstrip patch antenna design at 60 GHz confirmed by measurement results.

The reconfigurable antenna design is described in Section 2. The antenna realization and experimental results are in Section 3. The control elements implementation is discussed in Section 4. Conclusions are made in Section 5.

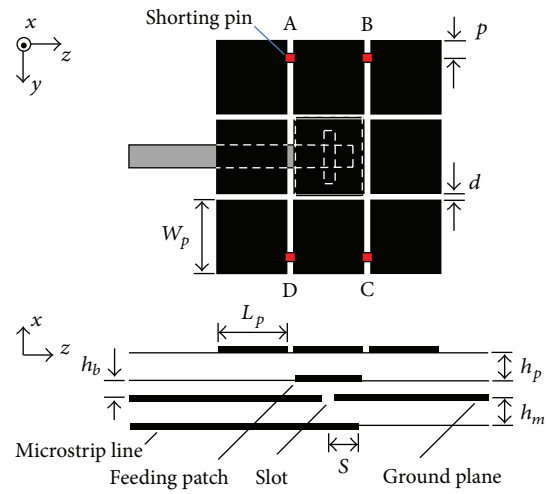

Figure 1: Top view and side view geometries of the reconfigurable aperture coupled stacked microstrip antenna with gridded parasitic patch.

2. Antenna Design

2.1. Antenna Geometry. The proposed reconfigurable antenna geometry top view and side view are shown in Figure 1. A detailed description of the antenna without switches is presented in [12]. The measured 10 dB return loss bandwidth for the antenna is from 54 GHz up to 67 GHz. The measured realized antenna gain is close to 8 dB [12]. The antenna has a three-layer structure. To form it a PTFE (polytetrafluoroethylene) substrate and a bonding film are used. A microstrip line is on the bottom side of the antenna. It feeds a single rectangular patch (feeding patch) using aperture coupling through a slot in the ground plane. The bonding film acts as a substrate for the feeding patch. On the top, there is a gridded parasitic patch formed by nine identical rectangular parts. The gridded patch is coupled electromagnetically to the feeding patch. In Table 1 the antenna design parameters are listed.

Shorting pins indicate switch positions for the reconfigurable antenna in Figure 1. There are four different positions, designated as A, B, C, and D. In the current realization switches are replaced by metal strips having 0.1 mm width. The pins are shifted on distance p from the antenna edge.

2.2. Beam Shift Realization. In this section simulation results from CST Microwave Studio are presented to investigate the behavior of the reconfigurable stacked microstrip antenna for different shorting pins configurations. The influence of the distance p is studied as well. The antenna model size is 5 mm by 5 mm. For the antenna pattern reconfigurability evaluation a term called total scan pattern is used. The evaluation method was introduced in [13] for antenna array performance analysis. The total scan pattern is obtained by evaluating, for each fixed angular direction, the largest gain in that direction of all different implementations of switches. In Figure 2 the antenna radiation pattern level graphs are shown in azimuth and elevation angle coordinates for 60 GHz. Azimuth is

Table 1: Stacked microstrip antenna design parameters.

Description	Value
Substrate Taconic TLY-5	$\epsilon_r = 2.2$, $\tan\delta = 0.0009$
Parasitic substrate thickness, h_p	0.127 mm
Microstrip substrate thickness, h_m	0.127 mm
Bonding film Arlon CuClad 6700	$\epsilon_r = 2.35$, $\tan\delta = 0.0025$
Bonding film thickness, h_b	0.0762 mm
Microstrip line width	0.375 mm
Microstrip line stub, S	0.50 mm
Slot length	0.20 mm
Slot width	0.85 mm
Feeding patch length, L_f	1.10 mm
Feeding patch width, W_f	1.29 mm
Parasitic patch length, L_p	1.16 mm
Parasitic patch width, W_p	1.20 mm
Parasitic patches separation, d	0.10 mm

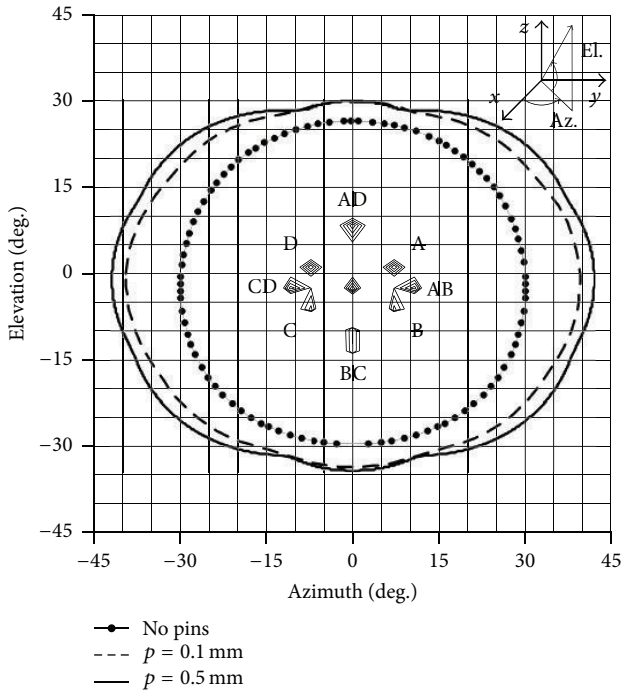

Figure 2: Antenna radiation pattern level graph for different configurations of shorting pins at 60 GHz. In the center of the graph normalized radiation patterns are shown for $p = 0.5$ mm with minimum level −0.02 dB. Outer graphs show realized gain level of radiation pattern for the reference antenna (no pins) and for the reconfigurable antenna total scan patterns when all possible shorting pins configurations are applied. Realized gain levels correspond to −3 dB from the reference antenna maximum realized gain.

the angle between an xy plane projection of a vector to a radiation pattern point and the x-axis. Elevation is the angle between a vector to a radiation pattern point and the xy plane. In the central part of the graph there are normalized radiation patterns for the antenna without shorting pins, or

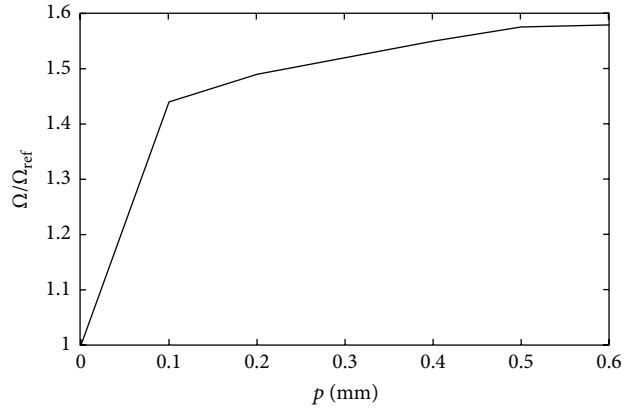

Figure 3: Relative beam coverage solid angle comparison for −3 dB level for the reference antenna ($p = 0$ mm) and for the reconfigurable antenna with different shorting pins distances from the antenna edge.

reference antenna (corresponding to a configuration when all switches are in "OFF" state), and for different combinations of shorting pins placed at $p = 0.5$ mm. Configuration A, for example, corresponds to a state when only shorting pin A is present or alternatively when switch A is in "ON" state and switches B, C, and D are in "OFF" state. Normalized patterns scale is from 0 dB to −0.02 dB. The purpose of such a representation is to show the position of the antenna beam maximum direction. Outer graphs in Figure 2 show realized gain level for the reference antenna radiation pattern and for the reconfigurable antenna total scan pattern, when all possible shorting pins configurations are applied. Realized gain level corresponds to −3 dB from the reference antenna maximum realized gain. For the comparison cases with $p = 0.1$ mm and with $p = 0.5$ mm are presented. The purpose of these graphs is to show the increase in the reconfigurable antenna beam coverage.

Figure 3 shows the computed beam coverage solid angle for realized gain level of radiation pattern for the antenna with different beam shift realizations; the common realized gain level of −3 dB from the reference antenna maximum realized gain is considered. The solid angle for the reference antenna realized gain (this corresponds to $p = 0$ mm) is taken as unit and is compared to the solid angle for the reconfigurable antenna total scan pattern level for different shorting pins distances from the antenna edge. It can be seen from the graph that it is possible for the beam coverage solid angle to increase from about 1.4 times for $p = 0.1$ mm to about 1.6 times for $p = 0.5$ mm. Further increase in distance p increases the solid angle just slightly; however the antenna return loss becomes much worse. Figure 4 shows the reconfigurable antenna reflection coefficient for different beam shift scenarios. The worst case is for the E-plane beam shift for $p = 0.5$ mm, where the return loss has about 8 dB level and there is a slight shift to higher frequencies. However, the antenna preserves wide bandwidth for all configurations.

The results for the reconfigurable antenna beam parameters for $p = 0.5$ mm are summarized in Table 2. The reference antenna beam has a small shift in the elevation angle due to

Table 2: Reconfigurable antenna simulated pattern parameters.

Switch				Position (degree)		Gain {realized gain} (dB)	Beam width (degree)		Effic. (%)
A	B	C	D	Az.	El.		Az.	El.	
				0	−2	9.4 {9.4}	60	56	95
ON	ON			11	−2	8.8 {8.7}	71	58	94
		ON	ON	−11	−2	8.8 {8.7}	71	58	94
	ON	ON		0	−12	8.4 {7.9}	76	63	93
ON			ON	0	8	8.2 {7.7}	76	65	92
ON				7	2	8.9 {8.8}	68	58	94
	ON			7	−7	9.0 {8.9}	68	58	94
		ON		−7	−7	9.0 {8.9}	68	58	94
			ON	−7	2	8.9 {8.8}	68	58	94

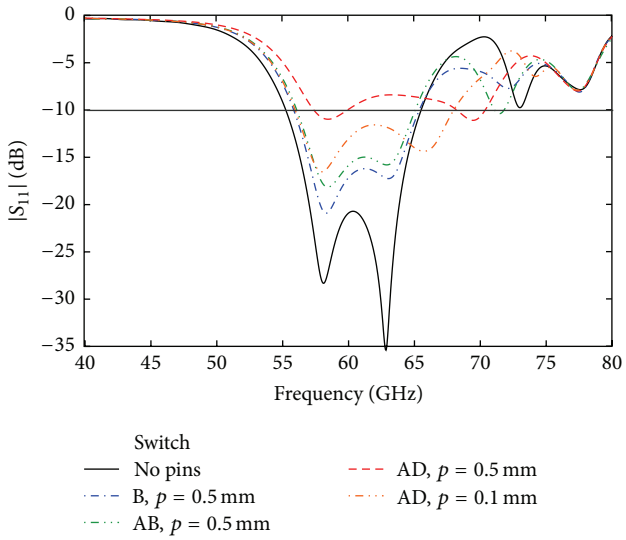

Figure 4: Reflection coefficient comparison for the reference antenna and for the reconfigurable antenna with different beam shift configurations.

the antenna asymmetry caused by the microstrip line. This shift further occurs for all the shorting pins configurations. Configurations AB and CD shift the antenna beam on 11° in azimuth plane; this corresponds to the antenna H-plane. Configurations AD and BC shift the antenna beam on 10° (with respect to the reference antenna) in the elevation plane; this corresponds to the antenna E-plane. Configurations A, B, C, and D shift the antenna beam in the diagonal plane, however more in the azimuth plane than in the elevation plane. The highest gain drop is for the E-plane beam shift and is 0.8 dB. The corresponding realized gain drop is 1.7 dB; this demonstrates worse impedance matching for the E-plane beam shift. The antenna efficiency remains nearly the same and it is more than 90% for all configurations. The beam width for all the shifted beams is wider, and this results in the antenna beam coverage increase.

Figure 5 shows a comparison for simulated absolute value of the electric field distribution at 60 GHz at the top surface of the reference antenna and antennas with different beam shift configurations for $p = 0.5$ mm. In the reference antenna the electric field phase on the top layer central patch is different from the phase of outer patches. The antenna top layer excitation is caused by the feeding patch on the lower substrate level. As the feeding patch size is comparable with the single part in the top layer grid, the central patch in the grid is excited first. Then due to the capacitive loading the excitation appears slightly later at the outer patches of the grid. The symmetrical arrangement of the patch grid generates radiation in the broadside direction. However, by using shorting pins in the grid, it is possible to introduce an asymmetry in the radiation aperture. In the antenna AB configuration, shown in Figure 5, three outer patches in the grid are connected by shorting pins and thereby have weak excitation. These patches act as a reflector for the electromagnetic field and the electric field amplitude is higher on remaining patches, when compared to the reference antenna. Due to the different excitation phase for the central patch and for side patches, the antenna maximum radiation is shifted from the broadside direction in the antenna H-plane. As follows from Figure 4 and Table 2, the antenna AB configuration preserves the impedance matching and efficiency; that is, the antenna radiated power is roughly the same as for the reference antenna and the gain drop in the antenna shifted beam is compensated by an increased beam width. Similar explanations apply to the beam shift in the antenna E-plane for the AD connection configuration and the beam shift in the antenna diagonal plane for the A connection configuration.

3. Measurement Results

Photos of the fabricated antenna samples fragments are shown in Figure 6. The sample with AB interconnections was fabricated with $p = 0.5$ mm; the interconnection width was 0.1 mm. Samples with AD and D interconnections were not fabricated initially and were obtained from the reference antenna using ribbon bonding. It was realized that manual procedure for a wire placement makes it difficult to put a wire exactly at $p = 0.5$ mm, and it was decided to make a ribbon bonding somewhere close to the patch edge. The sample with AD interconnection and the sample with D interconnection were roughly made with $p = 0.1$ mm. The wire width for

Table 3: Measured and simulated patterns parameters.

Switch	Position (degree) Meas. {Sim.}		Realized gain (dB) Meas. {Sim.}	Beam width (degree) Meas. {Sim.}	
	Az.	El.		Az.	El.
No pins (reference antenna)	0 {0}	7 {9}	7.8 {8.4}	57 {59}	55 {57}
AB (H-plane shift sample)	14 {10}	7 {9}	6.7 {7.4}	72 {73}	59 {61}
AD (E-plane shift sample)	0 {0}	19 {20}	6.6 {7.3}	75 {77}	58 {62}
D (D-plane shift sample)	2 {9}	8 {9}	7.1 {8.0}	60 {67}	64 {67}

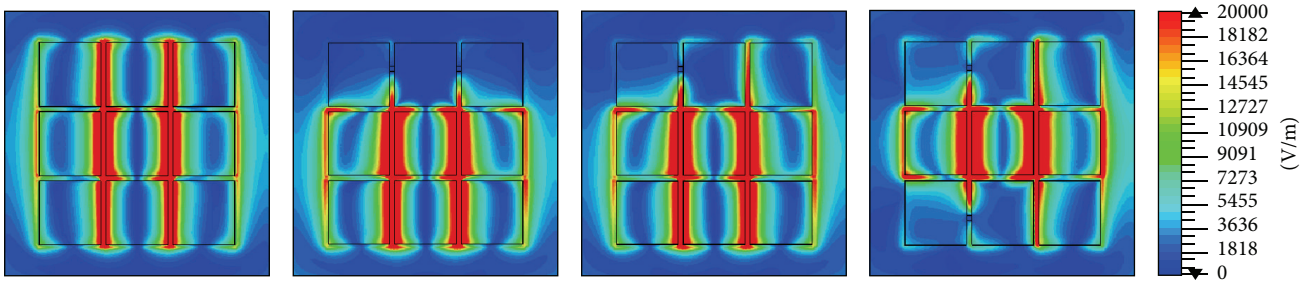

Figure 5: Simulated absolute value of the electric field distribution at 60 GHz at the antenna top surface for the reference antenna and antennas with different beam shift configurations with $p = 0.5$ mm. The total antenna substrate size is 5 mm by 5 mm.

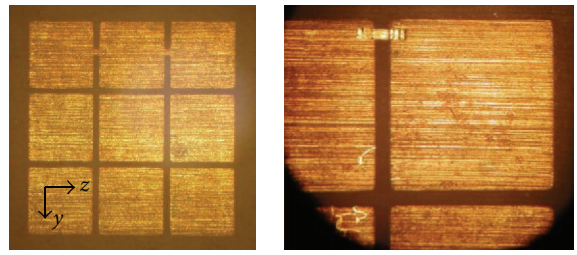

Figure 6: Photos of the fabricated antenna samples fragments. (a) is the sample with fabricated interconnections for $p = 0.5$ mm. (b) is the sample with ribbon bonding connection for $p = 0.1$ mm. The antenna total substrate size is 20 mm by 40 mm.

the performed ribbon bonding was 0.075 mm, which specified the interconnection width. According to performed simulations the interconnection width decrease in this case will have only minor influence on the antenna performance.

The samples were measured using a 1.85 mm end launch connector. To be able to attach the connector and to decrease its influence on measurements, the antenna sample size was made 20 mm by 40 mm. A connector model was made in CST and was used in combination with the antenna model to verify measurements. More information about radiation pattern and realized gain measurements can be found in [12].

Figure 7 shows the normalized pattern measurements for 60 GHz. The H-plane shift sample corresponds to AB interconnections. The E-plane shift sample corresponds to AD interconnections, and the D-plane shift sample corresponds to D interconnection. The measured and simulated results are summarized and compared in Table 3. It can be seen from the table that achieved beam shift angle is 14° for the H-plane shift sample with 1.1 dB realized gain drop compared to the reference antenna and 12° for the E-plane shift sample with 1.2 dB realized gain drop. Although the maximum radiation angle for the D-plane sample is not shifted significantly as it was expected, there is a clear pattern shift in Figure 7. For all the measured beam shift samples there is an increase in beam width meaning increased antenna beam coverage. The simulated results from Table 2 are different since the fabricated sample model takes into account the influence of a connector and different substrate size. The connector influence can be clearly seen on the E-plane radiation patterns, which are not symmetrical, and there are considerable ripples. The reason for this is an influence of a surface wave radiation and radiation from a connector, as discussed in [12]. This is why the effect from interconnections in the antenna is not well defined for E-plane patterns. However, good results agreement between simulation and measurements gives a reason to state that for AD and D interconnection the antenna without connector influence will behave in the same way as was shown in the previous section. The sample with D

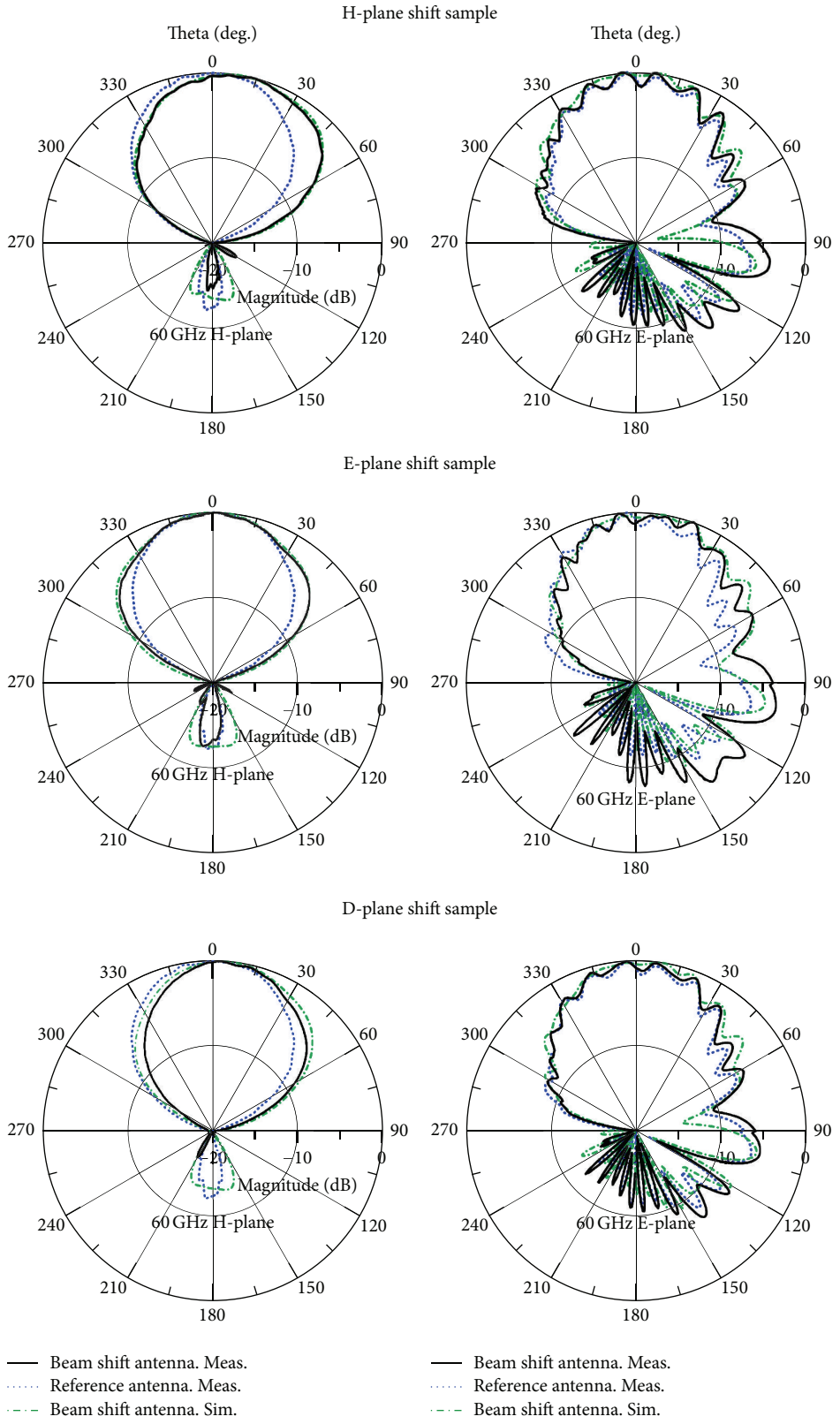

Figure 7: Normalized measured radiation patterns at 60 GHz for the reference antenna compared with measured and simulated radiation patterns for samples with beam shift. Patterns presented in the reference antenna H-plane and E-plane.

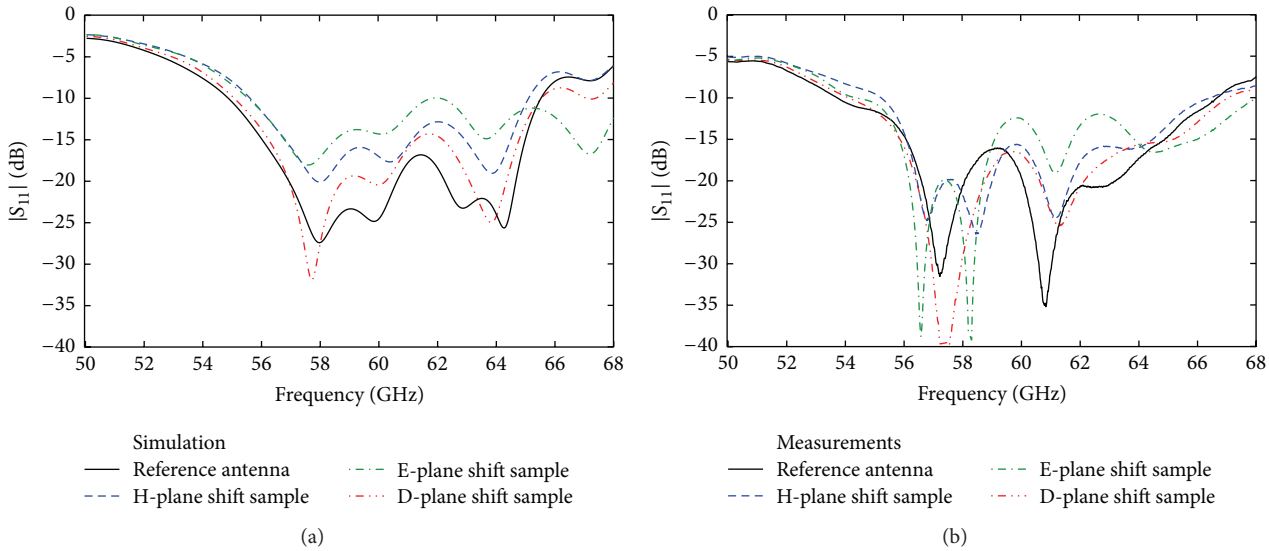

Figure 8: Simulated (a) and measured (b) reflection coefficient for the reference antenna (without shorting pins) and for samples with beam shift.

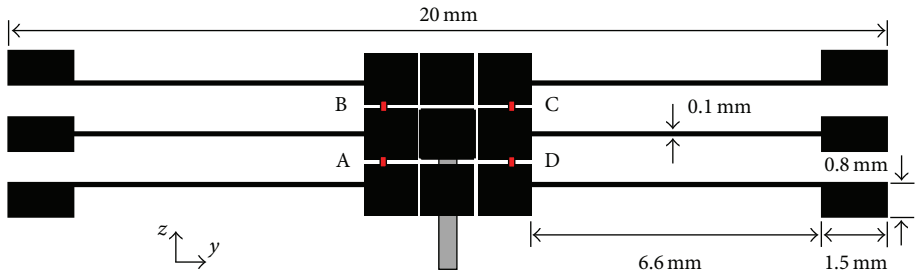

Figure 9: Fragment of the top layer geometry for the antenna with bias lines feeding network. The antenna total substrate size is 20 mm by 40 mm.

interconnection has worse agreement with the simulation perhaps because of no good ribbon bonding connection. The antenna patterns at 57 GHz and 64 GHz (not included for brevity) show only slight deviations compared to the pattern at 60 GHz. The measured cross polarization level for the reconfigurable antenna is roughly the same as for the reference antenna and it is below −20 dB for a normalized radiation pattern [14].

Figure 8 shows comparison for simulated and measured reflection coefficient. It can be seen from the graphs that all beam shift samples have approximately the same 10 dB return loss bandwidth as the reference antenna sample. This wide bandwidth covers entirely 60 GHz communication band.

4. Control Elements Implementation Consideration

In this paper, the connections are modeled by metal strips and should be considered as a prototype for a further realization using p-i-n diodes, the applicability of which has been proven in [11]. An alternative control element can be RF MEMS switches. The reason for using metal strips is to investigate the pure effect of interconnections and to separate it from different realizations of connecting switches. This is critical at higher frequencies where it is difficult to predict all the parasitic effects. Moreover, to mount a control component specified for high frequencies is nontrivial.

4.1. Feeding Network Implementation. Simulations show that thin bias lines, on the order of 0.1 mm, can be connected to the outer patches in the radiating grid with little impact on the field distribution by following two basic principles: the lines should be oriented along the y-direction defined in Figure 1 (orthogonal to the dominating electric field), and they should be connected to the center of the patches, where the amplitude of the electric field is low according to Figure 5.

In this section, a case of a bias lines feeding network implementation is considered for the fabricated antenna sample having dimensions 20 mm by 40 mm. Figure 9 shows the top layer geometry for the antenna with DC feeding network. The bias lines connect the antenna to the metal pads on the substrate edge, where external wires can be connected by soldering. The size of the metal pads is chosen to allow for manual soldering. Figure 10 shows the simulated absolute value of the electric field distribution at 60 GHz for the sample with DC feeding network. The metal pads and

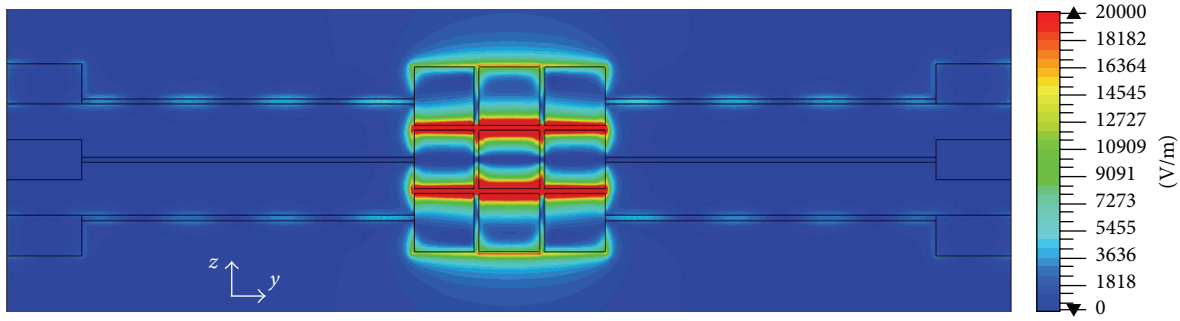

Figure 10: Simulated absolute value of the electric field distribution at 60 GHz at the top surface for the antenna with bias lines feeding network. The antenna total substrate size is 20 mm by 40 mm.

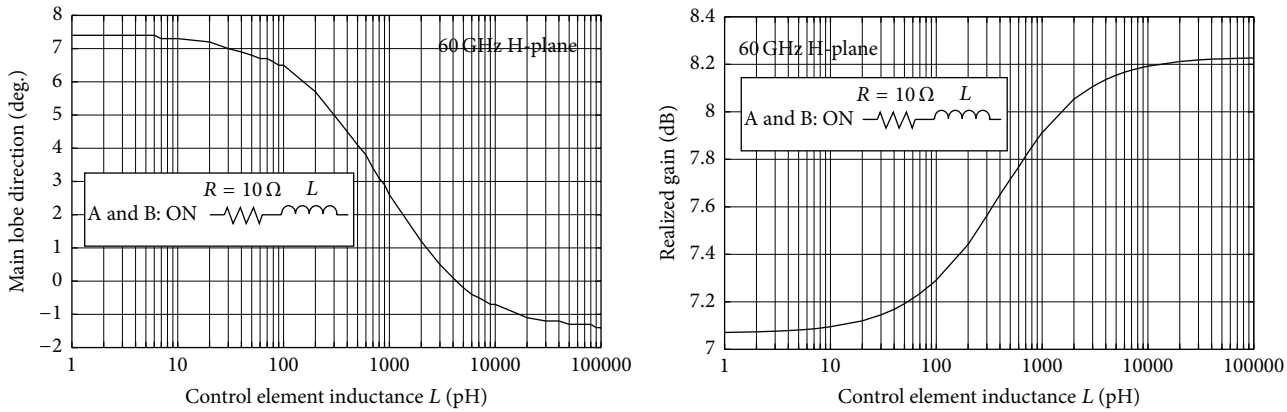

Figure 11: H-plane radiation pattern main beam direction (a) and realized gain (b) at 60 GHz for the reconfigurable antenna with A and B control elements in "ON" state.

the bias lines connected to the antenna center have negligible electric field excitation. The bias lines connected to bottom and top patches (according to Figure 10) in the antenna grid are slightly shifted from the corresponding patches center to have a minimum influence on the antenna radiation. Though there occurs some electric field leakage to the bias lines, the effect on the antenna performance is not considerable. The simulated realized gain difference between the antenna without and with bias lines and metal pads is 0.1 dB at 60 GHz.

4.2. Control Elements Investigation. The parasitics of the switches, such as on-resistance and off-capacitance of p-i-n diodes, can to some extent be included in the simulations using circuit models from the data sheets. However, these models are not always validated at frequencies as high as 60 GHz, and further parasitic effects associated with the mounting are expected. The parasitics are expected to influence the performance of the reconfigurable antenna, which may require some further design iterations.

A p-i-n diode used as a switch has to have two defined states: "ON" state and "OFF" state. The "ON" state is often represented by an inductor L in series with a low ohmic resistor R, typically having a resistance about 10 Ω, and the "OFF" state is represented by a capacitor C in series with an inductor L [6, 8, 11]. In this section, simulation results are presented aiming at investigating boundaries for resistance, inductance, and capacitance for the "ON" and "OFF" states of the control element. The reconfigurable antenna model has substrate size 20 mm by 40 mm and includes the bias lines feeding network described in the previous section and lumped circuit elements.

We assume the inductance can be taken to be the same in both states. To determine the inductance, we first consider a structure having only control elements A and B in the "ON" state, modeled by an inductor in series with a 10 Ω resistor, whereas control elements C and D are absent (perfect "OFF" state); see Figure 9. Figure 11(a) shows the main lobe direction in the antenna H-plane at 60 GHz, when varying the control element inductance. For inductance values less than 100 pH the antenna radiation pattern is shifted in the H-plane by approximately 7°. This indicates the state when control elements A and B work as shorting pins. This behavior occurs when the inductor absolute value impedance at 60 GHz is comparable to 10 Ω resistance. For inductance values larger than 10 nH, the control elements A and B work as insulators. Figure 11(b) indicates a drop in realized gain at 60 GHz for the case when elements A and B are in "ON" states. The conclusion that can be made from these results is that

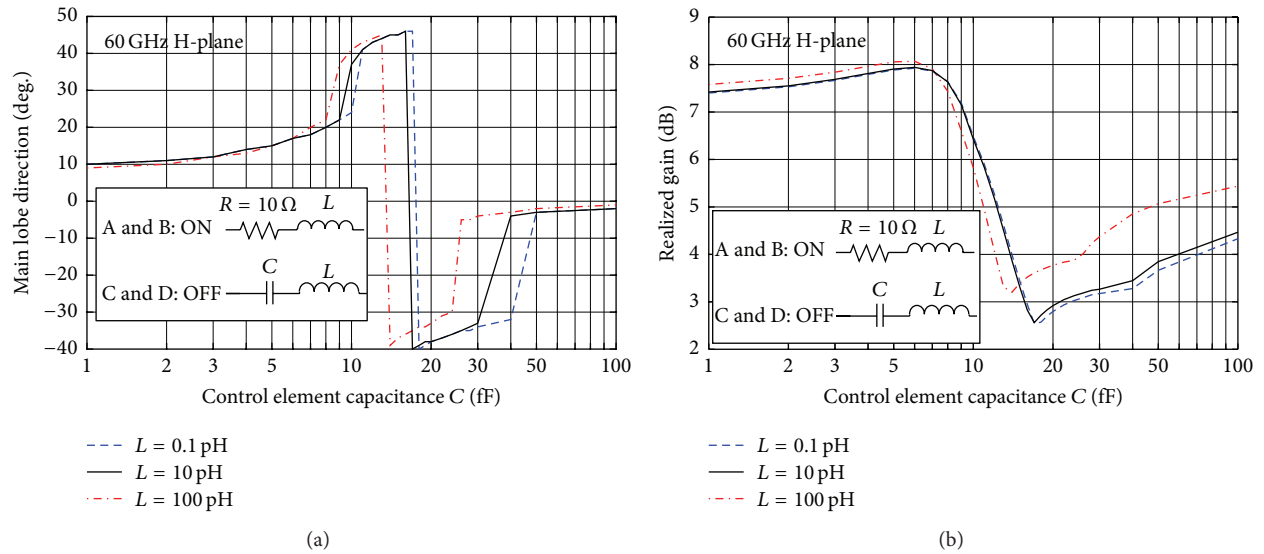

FIGURE 12: H-plane radiation pattern main beam direction (a) and realized gain (b) at 60 GHz for the reconfigurable antenna with A and B control elements in "ON" state, together with C and D control elements in "OFF" state.

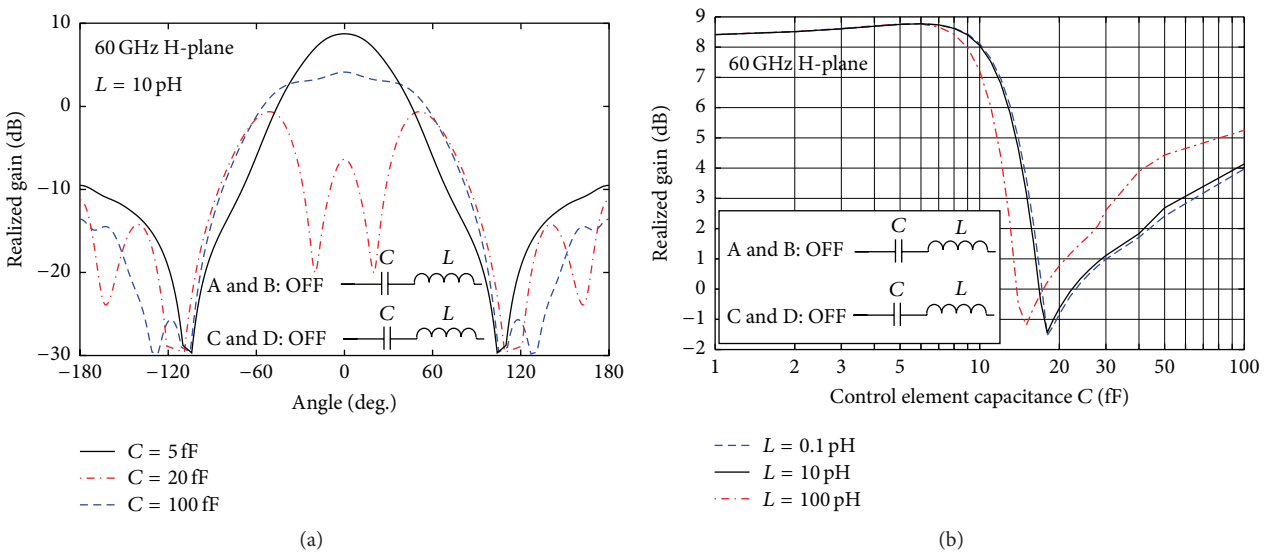

FIGURE 13: Radiation patterns in the antenna H-plane (a) and realized gain (b) at 60 GHz for the reconfigurable antenna with A, B, C, and D control elements in "OFF" state.

the preferable inductance for the control element value should be less than 100 pH.

The next step is to study the capacitance of the "OFF" state. We consider a structure where control elements A and B are in the "ON" state, and control elements C and D are modeled by an inductor in series with a capacitor, emulating the "OFF" state. Figure 12 shows the main lobe direction in the antenna H-plane and the realized gain at 60 GHz, for varying control element capacitance and three values of inductance. From these results it follows that the preferable capacitance value for the "OFF" state should be less than 10 fF. It can be noticed that for capacitance around 10 fF beam shift angle increases to about 40° with realized gain increase; however this state is not stable and needs precise capacitance control, and it is not clear that this can be achieved using p-i-n diodes. Instead varactors with proper range might be examined as candidates for control elements.

To complete the control elements investigation we consider the case when all of them are in "OFF" state. This case is assumed as a basic operational mode for the antenna with radiation in a broadside direction. Figure 13 shows radiation patterns in the antenna H-plane and the realized gain at 60 GHz, for varying control element capacitance and three values of inductance. In contrast to the two operational modes discussed above, in case when all the control elements are in "OFF" state, the antenna radiation aperture is symmetric in the antenna H-plane, and the main lobe direction graph is not relevant. From the results presented in Figure 13

the same recommendation for the capacitance value follows, as was made for the previous case. The preferable capacitance value for the "OFF" state should be less than 10 fF. For this condition the antenna has the highest realized gain in the broadside direction, about 8.5 dB, and the antenna has good impedance matching. For the capacitance values between 10 fF and 20 fF there is a sharp drop for the antenna gain, with two dominating side lobes in the antenna radiation pattern. For this condition the contribution to the antenna radiation is mainly from the outer patches in the grid structure. For the capacitance values more than 50 fF the control elements work as shorting pins, and the contribution to the antenna radiation is mainly from the center patch in the grid structure. In this case the reconfigurable antenna realized gain is close to 5 dB, which roughly corresponds to the single microstrip patch antenna gain. However, the reconfigurable antenna impedance matching is poor in this mode.

5. Conclusion

A beam shift realization is presented for a novel wideband stacked microstrip antenna with gridded parasitic patch designed for 60 GHz central frequency. The beam shift is obtained by connecting adjacent rectangular patches forming a gridded parasitic structure. Connections are performed by using metal strips and considered as a prototype for p-i-n diodes or RF MEMS switches implementation on the antenna top layer. Nine different beam directions are realized. The reconfigurable antenna preserves wide bandwidth, about 13 GHz, for all beam shift scenarios. Measurement results are in good agreement with simulations. The measured beam shift angles are 14° and 12° in the H-plane and in the E-plane, respectively. Simulations show about 60% increase in the beam coverage solid angle for −3 dB level of radiation pattern for the reconfigurable antenna compared to the reference antenna. We believe that this would be a considerable improvement for a wireless communication system. The measured reference antenna gain is about 8 dB, whereas even short range communication might require more. The gain can be increased in several ways. A moderate increase is achieved by using the gridded parasitic patch antenna as a single element in an array antenna with only a few elements. More significant increase is achieved by making a larger array, or by using the antenna as a feed combined with a reflector or lens. The latter case may be necessary when considering millimeter-wave backhaul applications, where about 30 dB gain is desired.

Simulation confirms high efficiency for the reconfigurable antenna. The 5 mm by 5 mm model has more than 90% efficiency for all the antenna configurations, although this is expected to be an overestimation compared to the manufactured antenna.

A realistic control element implementation is investigated. Simulations show that the bias lines implementation has negligible effect on the reconfigurable antenna performance. For p-i-n diodes implementation as switches the preferable inductance for the "ON" and "OFF" states is less than 100 pH. The preferable capacitance for the "OFF" state is less than 10 fF. These values are challenging to find in commercial off-the-shelf diodes where the packaging introduces several parasitics and may require a high level of integration of the control elements in the manufacturing procedure in order to be realized.

Conflict of Interests

The authors declare that there is no conflict of interests regarding the publication of this paper.

References

[1] P. Smulders, "Exploiting the 60 GHz band for local wireless multimedia access: prospects and future directions," *IEEE Communications Magazine*, vol. 40, no. 1, pp. 140–147, 2002.

[2] S. Scott-Hayward and E. Garcia-Palacios, "Multimedia resource allocation in mmwave 5G networks," *IEEE Communications Magazine*, vol. 53, no. 1, pp. 240–247, 2015.

[3] F. Boccardi, R. W. Heath, A. Lozano, T. L. Marzetta, and P. J. Popovski, "Five disruptive technology directions for 5G," *IEEE Communications Magazine*, vol. 52, no. 2, pp. 74–80, 2014.

[4] R. Kalimulin, A. Artemenko, R. Maslennikov, J. Putkonen, and J. Salmelin, "Impact of mounting structures twists and sways on point-to-point millimeter-wave backhaul links," in *Proceedings of the IEEE International Conference on Communications Workshops (ICC '15)*, pp. 19–24, London, UK, June 2015.

[5] S. L. Preston, D. V. Thiel, J. W. Lu, S. G. O'Keefe, and T. S. Bird, "Electronic beam steering using switched parasitic patch elements," *Electronics Letters*, vol. 33, no. 1, pp. 7–8, 1997.

[6] M. Jusoh, T. Aboufoul, T. Sabapathy, A. Alomainy, and M. R. Kamarudin, "Pattern-reconfigurable microstrip patch antenna with multidirectional beam for WiMAX application," *IEEE Antennas and Wireless Propagation Letters*, vol. 13, pp. 860–863, 2014.

[7] S. V. S. Nair and M. J. Ammann, "Reconfigurable antenna with elevation and azimuth beam switching," *IEEE Antennas and Wireless Propagation Letters*, vol. 9, pp. 367–370, 2010.

[8] Z. Li, E. Ahmed, A. M. Eltawil, and B. A. Cetiner, "A beam-steering reconfigurable antenna for WLAN applications," *IEEE Transactions on Antennas and Propagation*, vol. 63, no. 1, pp. 24–32, 2015.

[9] H. V. Hunerli, H. Mopidevi, E. Cagatay et al., "Three dimensional microfabricated broadband patch and multifunction reconfigurable antennae for 60 GHz applications," in *Proceedings of the 9th European Conference on Antennas and Propagation (EUCAP '15)*, pp. 1–5, Lisbon, Portugal, April 2015.

[10] Y. Yang, K. Y. Chan, N. Nikolic, and R. Ramer, "Experimental proof for pattern reconfigurability of 60-GHz quasi-Yagi antenna," *Microwave and Optical Technology Letters*, vol. 57, no. 1, pp. 84–88, 2015.

[11] H. Kamoda, T. Iwasaki, J. Tsumochi, T. Kuki, and O. Hashimoto, "60-GHz electronically reconfigurable large reflectarray using single-bit phase shifters," *IEEE Transactions on Antennas and Propagation*, vol. 59, no. 7, pp. 2524–2531, 2011.

[12] A. Bondarik and D. Sjöberg, "Gridded parasitic patch stacked microstrip antenna with beam shift capability for 60 GHz band," *Progress in Electromagnetics Research B*, vol. 62, pp. 319–331, 2015.

[13] J. Helander, K. Zhao, Z. Ying, and D. Sjoberg, "Performance analysis of millimeter wave phased array antennas in cellular

handsets," *IEEE Antennas and Wireless Propagation Letters*, 2015.

[14] A. Bondarik and D. Sjöberg, "Investigation of reconfigurability for a stacked microstrip patch antenna pattern targeting 5G applications," in *Proceedings of the IEEE-APS Topical Conference on Antennas and Propagation in Wireless Communications (APWC '15)*, pp. 1202–1205, IEEE, Turin, Italy, September 2015.